Real-time monitoring of InAs/GaAs quantum dot growth using ultraviolet light scattering

T. Pinnington, Y. Levy, J. A. MacKenzie, and T. Tiedje*
Department of Physics and Astronomy, University of British Columbia, Vancouver, British Columbia, Canada V6T 1Z4
(Received 14 April 1999)

We present real-time measurements of surface structure evolution during quantum dot growth in InAs/GaAs grown by molecular-beam epitaxy. The measurements were made using an ultraviolet light-scattering technique in which the 254 nm line of a mercury lamp is used as the light source. This technique provides sensitivity to roughness on lateral lengthscales as low as 154 nm for our setup. Using this technique, we can detect the onset of quantum dot formation in this system, as indicated by reflection high-energy electron-diffraction measurements. The continuous increase in the scattering signal after the dots have formed, is explained in terms of diffusion-limited growth and ripening of the large islands that coexist with the quantum dots. [S0163-1829(99)09047-5]

I. INTRODUCTION

The performance of molecular-beam epitaxy (MBE)-grown structures in devices is critically affected by the morphology of the interfaces between the deposited layers. This is directly related to the surface roughness of the growing film. The roughness is often characterized by a particular length scale, which in MBE can range from tens of nanometers (typical average spacing of InAs quantum dots) to microns (correlation length of mounds formed in GaAs homoepitaxy). It is therefore important to have noninvasive *in situ* methods of monitoring surface roughness on these length scales, preferably in real time. The monitoring techniques traditionally available to MBE do not meet these requirements. Reflection high-energy electron diffraction (RHEED), for example, is sensitive to surface structure on the scale of a few tens of lattice constants, but due to its small coherence length cannot provide information on larger lengthscales, such as quantum dot size and density. Scanning tunneling microscopy (STM), on the other hand, is neither real-time nor noninvasive, since it requires interruption of the growth in which the sample is quenched for imaging.

In this paper we discuss *in situ* monitoring of quantum dot growth using ultraviolet elastic light scattering (UVLS). Light scattering is a noninvasive technique that is directly sensitive to the power spectral density (PSD), of the surface morphology.[1] The measured spatial frequency q depends on the incident and scattered angles and the wavelength λ of light used, and is related to a lengthscale L in the plane of the surface by $q=2\pi/L$. Spatial frequencies as high as $2\pi/\lambda$ are accessible by monitoring backscattered light at grazing incidence. The two-dimensional PSD has units of (length) to the fourth power, and can be thought of as the square of the rms roughness at a particular q per unit spatial frequency range $dq_x dq_y$. Thus the light-scattering signal has a precise interpretation in terms of the statistical properties of the surface roughness. Compared to other *in situ* monitors of surface structure (RHEED, STM), light scattering is inexpensive and straightforward to implement on existing deposition systems. The scattering signal represents a spatial average over the illuminated surface area, so that statistical topographic information of large areas (typically $>\mathrm{mm}^2$) is obtained. Light scattering has been used successfully by several groups to monitor thin-film surface roughness in real time during growth and recently has been used to obtain quantitative information on thin-film growth dynamics, during strain relaxation in InGaAs heteroepitaxy and island formation in SiGe on Si, for example.[2,3]

In the present work we have developed an *in situ* light-scattering apparatus using the 254 nm line of a mercury lamp as the light source, which can monitor roughness on much smaller lengthscales than can be observed using visible wavelengths. We have applied this tool to the study of a system of intense technological and scientific interest, namely the growth of InAs quantum dots on (100) GaAs.[4–6] We find that high sensitivity to small lengthscale roughness as provided by UVLS is crucial in detecting the roughness associated with quantum dot formation, above the background roughness of the substrate. With our setup, we can detect roughness corresponding to a power spectral density of 1 nm^4, at a spatial frequency of 41 $\mu\mathrm{m}^{-1}$ (lengthscale of 154 nm). This would correspond, for example, to a minimum detectable quantum dot density of ~ 1 $\mu\mathrm{m}^{-2}$ (1×10^6 cm^{-2}), for 8 nm height quantum dots, assuming the spatial distribution of the dots is approximately random. The light-scattering signal increases continuously during annealing of the quantum dots, which we attribute to the growth and ripening of the large islands that coexist with the dots. During the late stages of annealing, the scattering signal is approximately proportional to $n\langle V\rangle^2$, where n is the island density and $\langle V\rangle$ is the average island volume. Thus it is possible to extract structural information about the large islands in real time during annealing. The sensitivity can easily be improved by using a more intense light source such as a UV laser. To our knowledge no other real-time studies of the structural evolution of quantum dots in III-V systems have been reported.

II. EXPERIMENT

The InAs quantum dot growth experiments were carried out in a VG-V80H MBE deposition system, equipped with solid-source effusion cells for both group III and group V elements. RHEED was used to monitor the two-dimensional

(2D) to three-dimensional transition associated with the quantum dot formation. The substrate temperature was monitored throughout growth using a diffuse reflectance spectroscopy (DRS) apparatus, which has an absolute accuracy of $\sim 10\,^{\circ}\mathrm{C}$.[7] All of the growths were on nominally on-axis ($\pm 0.5\,^{\circ}$) (001)-oriented GaAs substrates. Prior to loading into the MBE system, the substrates were oxidized by exposure to UV ozone, to move surface contaminants away from the oxide/GaAs interface. In order to minimize particulate contamination that would interfere with the light-scattering measurements, no wet chemical treatments were performed on these epi-ready substrates. The wafers were then transferred to the MBE growth chamber and heated to $600\,^{\circ}$ C under As_2 overpressure to evaporate the oxide. This was followed by growth of a 1 μm thick GaAs buffer layer at $600\,^{\circ}\mathrm{C}$, during which the surface roughness dropped to the level of the starting substrate over the spatial frequency range of interest, as measured by light scattering. During the final 10 min of buffer layer growth the substrate temperature was ramped down to below $500\,^{\circ}\mathrm{C}$ in preparation for the InAs deposition. A 5 to 10 min growth interrupt was required immediately prior to the dot growth to allow the arsenic flux and substrate temperature to stabilize at the desired settings. Nominally three monolayers of InAs were deposited at a growth rate of ~ 10 ML/min, under an As_2 overpressure at the substrate of $\sim 5\times 10^{-7}$ mbar. The onset of quantum dot formation was signaled by the transition from a streaky RHEED pattern associated with a 2D growth front, to a spotty pattern indicative of 3D growth.[9] Following deposition of the InAs, the substrate temperature was held fixed so that the time-evolution of the quantum dots during annealing could be observed. After the annealing experiment was concluded, the substrate heater power was shut off to quench the sample by radiative cooling to the liquid-nitrogen filled cryoshroud. Samples were then removed from the growth chamber and characterized by *ex situ* atomic-force microscopy (AFM).

Real-time monitoring of the quantum dot formation was accomplished using 254 nm wavelength light from a 100 W Hg arc lamp. Light was incident at an angle of $55\,^{\circ}$ relative to the sample normal, through a viewport located at a vacant effusion cell position. The light from the $\sim 0.3 \times 0.3$ mm^2 arc was spatially filtered using UV optics so that an estimated 10^{-3} W of 254-nm emission was focused to a clean, ~ 50 mm^2 spot on the sample. The output power of the lamp was monitored using a silicon photodiode detector with a 254 nm line filter. Scattered light was detected at two positions by photomultiplier tubes, at a shutter port and a mass spectrometer quadrupole port, corresponding to backscattering in the plane of incidence at $-25\,^{\circ}$ and backscattering $23\,^{\circ}$ out of the plane at $-60\,^{\circ}$ respectively. This configuration is sensitive to roughness at spatial frequencies of 31 and 41 $\mu\mathrm{m}^{-1}$. In addition, a 10 mW, 488 nm, *s*-polarized Ar ion laser beam was coupled into the chamber through the same viewport as the Hg arc lamp beam. The scattered 488 nm light was detected with a third photomultiplier tube at the $-25\,^{\circ}$ shutter port, permitting access to 16 $\mu\mathrm{m}^{-1}$ roughness. In this way three different spatial frequencies corresponding to roughness on lengthscales of 154, 205, and 393 nm were monitored simultaneously throughout the growth experiments.

Access for the UV light to the sample at the center of the MBE growth chamber was through heatable viewports with 25 mm diameter sapphire windows, which were cleaned by heating to $500\,^{\circ}\mathrm{C}$ after each growth. Arsenic deposits that accumulated on the windows at the detector positions during a single growth were invisible to the eye and did not significantly affect the scattering signal. Coating of the input window by contrast was dramatically enhanced over the input beam area. This window was therefore kept heated to $300\,^{\circ}\mathrm{C}$ throughout growth, which prevented any deposits from forming. Although we do not know the precise mechanism for the light-assisted window coating, *ex situ* AFM analysis of the films did not show any significant effect of the light on the dot growth. We note also that adlayer photolysis has been observed using 248 nm laser light during growth of InAs dots by metal-organic chemical vapor deposition, however much higher intensities (45 W/cm^2) were used.[8]

Because the surfaces of films produced by MBE are nearly specular (typically ~ 1 nm rms roughness over 10×10 μm^2, according to AFM), the light-scattering signal at far from specular angles as used here is many orders of magnitude less than the specular beam. Thus special care was taken to reduce the amount of stray light which entered the detector, for example by scattering of the specular beam from the chamber walls. In our setup, the specularly reflected light was diverted out of the growth chamber through a viewport at the specular position. Lock-in detection and optical line filters were used to remove noise arising from ambient light in the chamber from ion gauges and the DRS temperature measurement. The signal was maximized using a UV quartz lens to collect the light that scatters into the solid angle of the output window. This also has the effect of averaging out the speckle noise in the scattered light distribution. The collected light was spatially filtered at the input aperture of each photomultiplier tube detector to minimize the detection of light scattered from the edges of the sample. Care was taken to avoid contamination of the surfaces with particles that exhibit large backscatter,[10] which are easily detectable by eye. Growth experiments were not performed on wafers that contained particulate contamination within the area illuminated by the probe beam.

III. RESULTS

A. Real-time light scattering

In Fig. 1 we show the time evolution of three scattered light intensity signals acquired simultaneously during a quantum dot growth experiment. The dots were grown and annealed for 2 min at a substrate temperature of $490\,^{\circ}\mathrm{C}$ on a GaAs buffer layer prepared in the manner described above. The three signals correspond to measurements of the PSD of the surface at three different spatial frequencies, namely 16, 31, and 41 $\mu\mathrm{m}^{-1}$. For consistency, the plane of incidence was aligned approximately with a $\langle 100\rangle$ direction in the plane of the substrate for each growth experiment, however, based on AFM analysis of the samples the scattering signal during dot growth is expected to be isotropic. The signals have each been normalized at $t=0$ to the initial scattering intensity, which is the sum of any stray background light and the signal from the GaAs buffer layer. Nominally 3 ML of InAs were deposited in 0.3 min, starting at $t=0$. The 2D to 3D RHEED transition was observed at $t\sim 0.2$ min, which

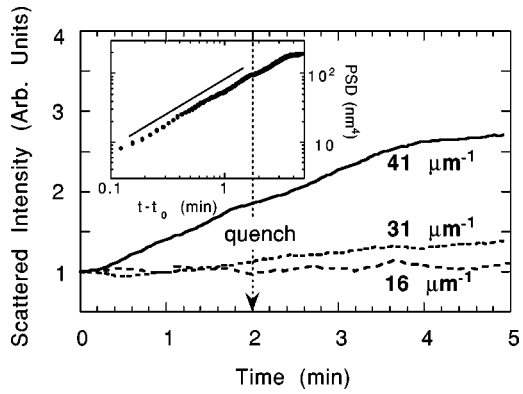

FIG. 1. Time evolution of the light-scattering signals during a quantum dot growth at 490 °C, with nominally 3 ML of InAs. The indium deposition was terminated at $t=0$, and the film was quenched at $t=2$ min (indicated by dashed line in the figure). Each scattering signal is normalized to unity at $t=0$. Inset: PSD calculated from the 41 μm^{-1} signal after subtracting the background, plotted on a log-log scale. The time t_o is 0.2 min and corresponds to the onset of islanding according to RHEED. The solid line has a slope of 1.

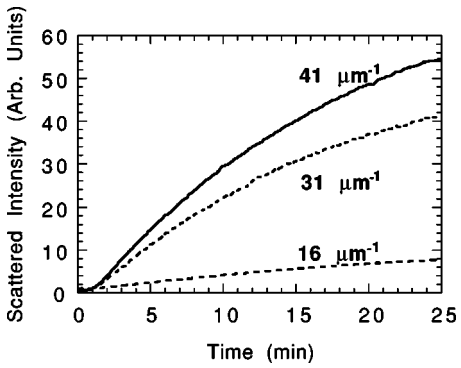

FIG. 2. Light-scattering signals during a dot growth and 25 min anneal at 400 °C. Nominally 3 ML of InAs was deposited. The three signals are normalized at $t=0$.

coincides with the onset of roughening observed in the light scattering at $q=41$ μm^{-1}. Based on the AFM structural analysis and discussions below, we attribute the increase in the scattering signal during the anneal to the growth of the small, self-limited structures referred to in the literature as quantum dots (QD's). Note that throughout the entire anneal, the signal at $q=16$ μm^{-1} did not increase sufficiently above the initial background scattering from the GaAs buffer to be discernible above the noise. Thus sensitivity to high spatial frequency roughness is critical for the monitoring of dot growth. Following the anneal the sample was quenched under arsenic overpressure as described above. The continued increase in the light-scattering signals indicates that the dots continued to evolve during the first two minutes of the quench, by which time the substrate temperature had dropped to 300 °C as measured by diffuse reflectance spectroscopy.

In order to examine the effect of annealing, other experiments were performed with longer annealing times. It was found that annealing for extended periods at 490 °C resulted in evaporation of the InAs dots, during which a 2D RHEED pattern was recovered and the light-scattering signals decayed to their initial values. In Fig. 2 we show results obtained during an anneal at a substrate temperature of 400 °C, where evaporation of InAs is not significant. Other than the substrate temperature, all growth parameters were nominally identical to those used in the dot growth above. We note that all three signals increase during the anneal, although the relative increase is much greater at the higher spatial frequencies. Again, this increase in the scattered light intensity is associated with QD formation and the subsequent appearance of larger islands. The continued increase observed during the late stages of annealing is attributed to Ostwald ripening[11,12] of the larger islands, as has been observed previously.[5,13]

B. Analysis of AFM data

In Figs. 3 and 4 we show *ex situ* AFM images (Tapping mode, Digital Instruments Multimode AFM) of the quenched samples following deposition of a GaAs buffer layer [Fig. 3(a)], after the quantum dot growth at 490 °C described above [Figs. 3(b) and 3(c)], and after a similar growth in which the sample was annealed for 25 min at 440 °C [Fig. 3(d), and Fig. 4]. The 2D isotropic power spectra obtained from Fourier transforms of Fig. 3(a), and a 10×10 μm^2 image of the film in Fig. 3(c), are shown in Fig. 5. The buffer layer displays mounds elongated along [011], which are characteristic of MBE GaAs growth on GaAs substrates prepared using thermal oxide desorption.[14] The PSD of this film [Fig. 5, curve *b*] exhibits a power-law dependence on spatial frequency, which was also observed in *ex situ* light-scattering measurements on GaAs buffer layers.[15] The finite radius of the AFM tip is known to produce artifacts in the PSD obtained from AFM.[16] In order to verify that these ef-

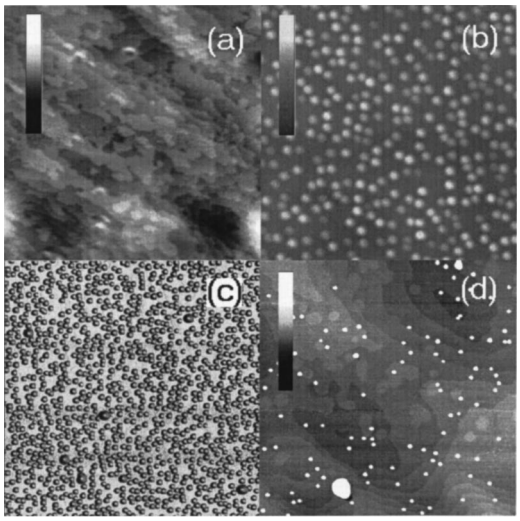

FIG. 3. AFM images taken at various stages of the dot growth. The [010] crystal direction is approximately parallel to the slow scan axis (y axis) in each image. (a) A GaAs buffer layer (scan size $=2\times2$ μm^2, grayscale = 4 nm), (b) the quantum dot distribution from the growth in Fig. 1 (1×1 μm^2, 30 nm grayscale), (c) 2×2 μm^2 image (illumination mode) of the film in Fig. 1, showing both the QD's and the large islands, and (d) 2×2 μm^2 image (grayscale = 10 nm) showing QD's and large islands after a 25 min anneal at 440 °C. The grayscale has been adjusted to reveal the underlying surface steps, so that the dots appear saturated white in this image.

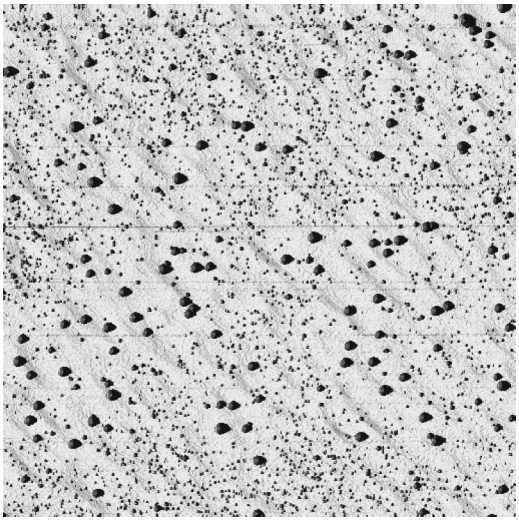

FIG. 4. Large scale (20×20 μm^2) illumination-mode image of the film in Fig. 3(d), showing the spatial distribution of the QD's and the large islands.

fects are not important in this case we have compared AFM data with simulated data in which the steps in the original image are replaced with steps having abrupt edges, perfectly flat terraces, and uniform step height equal to the (100) lattice spacing. We find that the PSD obtained from AFM is identical to the simulated data if the steps are well resolved by the AFM, as is the case for Fig. 3(a). The observed power law of the PSD in this film is approximately -3. In general, we find that GaAs buffer layers grown under these conditions exhibit power-law behavior which falls in the range of -2.5 to -3. This means that the surface morphology of the starting buffer layer is self-affine.[17]

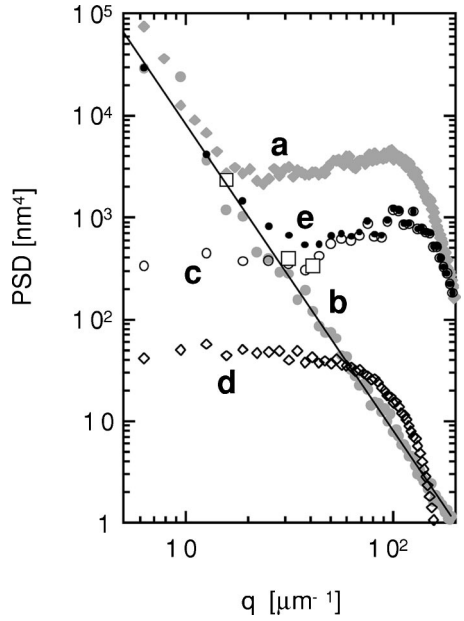

FIG. 5. Estimation of the 2D PSD of the QD and large island distributions resulting from the growth in Fig. 1, based on post-growth AFM. (a) Grey diamonds, PSD calculated directly from the Fourier transform of a 10×10 μm^2 AFM scan of the film. (b) Grey circles, PSD of the AFM image of the bare GaAs buffer layer in Fig. 3(a). The solid line has a slope of -3. (c) Open circles, PSD for a simulated QD distribution, in which each dot in Fig. 3(b) was replaced with a cone as discussed in the text. (d) Open diamonds, PSD of a large island distribution obtained by replacing the 37 large islands in the AFM scan used in (a) with 1:2 aspect ratio cones. (e) Solid black circles, estimate of the true PSD of the film measured by AFM in (a), obtained by adding the PSD curves obtained in (b), (c), and (d). As discussed in the text, the three open squares are an independent estimate of the true PSD from light scattering, evaluated at the three spatial frequencies in Fig. 1.

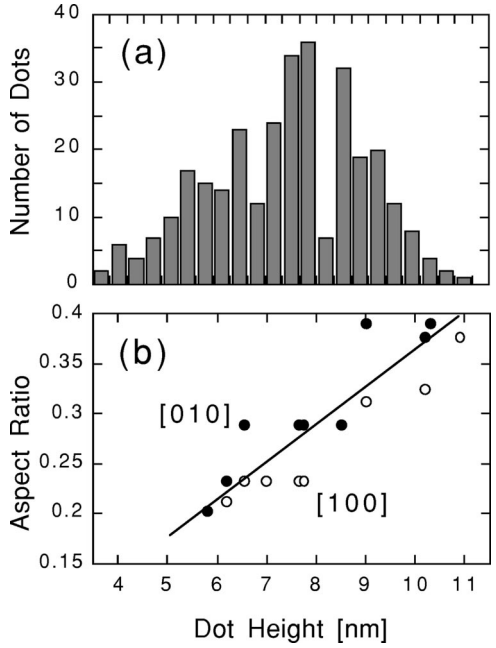

FIG. 6. (a) Quantum dot height distribution for the growth at 490 °C, determined from the AFM data in Fig. 3(b). (b) Inferred aspect ratio of the QD's, based on simulated AFM profiles as shown in Fig. 7.

Small-scale and large-scale images of the quantum dot distribution produced in the growth in Fig. 1 are shown in Figs. 3(b) and 3(c), respectively. The images reveal two distinct populations of dots. The heights of the smaller dots, which have a density of 3.0×10^2 μm^{-2}, are distributed as shown in Fig. 6(a), based on a sample size of 308 dots. The mean and standard deviation of the height of the dots are 7.5 ± 0.1 nm and 1.6 nm, respectively. A similar analysis on 37 of the larger dots yielded a mean height, standard deviation and density of 19.5 ± 0.5 nm, 3 nm and 0.3 μm^{-2}. Bimodal size distributions are commonly found in this and other strained-island systems.[5,18,21] The smaller dots (QD's) are believed to be self-limiting in size whereas the larger dots are found to grow during prolonged annealing, possibly due to the incorporation of a defect such as a dislocation, which removes the self-limiting constraint.[5] These larger structures which continue to grow will be referred to in this paper as large islands, in order to differentiate them from the QD's. The PSD calculated from a 10×10 μm^2 image of the film in Fig. 3(c) is plotted in Fig. 5 (curve a). For low spatial frequencies ($q<20$ μm^{-1}), we see the same roll-off behavior as for the bare buffer layer, however for higher frequencies the PSD remains approximately constant with q. The roll-off above $q>100$ μm^{-1} is due entirely to the finite diameter of the dots as imaged by AFM, as discussed below. The dramatic increase in roughness at small length scales

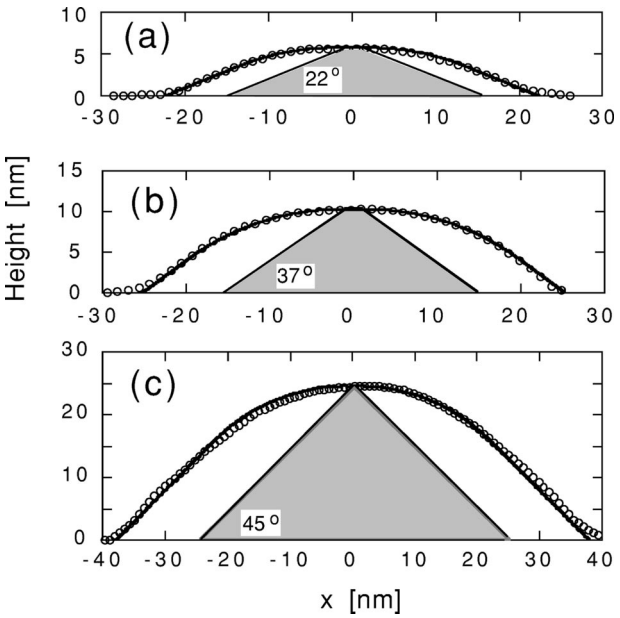

FIG. 7. Comparison of three simulated AFM scan profiles (solid line) with actual AFM measurements from Fig. 3(c) (open circles), for two QD's having heights of (a) 5.8 nm, (b) 10.3 nm, and one large island of height 24.6 nm (c). The AFM measurements were taken approximately along the [010] direction, through the center of each island. The solid curves simulate the scanning of a 30 nm radius probe tip over the truncated triangle shown, whose aspect ratio was adjusted to optimize the fit with the AFM data.

following quantum dot growth explains the enhanced sensitivity of the high spatial frequency light-scattering signals.

The dot distributions change considerably during annealing, as shown by the AFM images in Fig. 3(d) and Fig. 4 for the sample annealed for 25 min at 440 °C. We note that the small dots have the same average size as those in Fig. 3(c), as expected for QD's. By contrast the size of the large islands has increased dramatically (typical height of 50 nm) during the anneal. We note that the large islands in both Fig. 3(c) and in Fig. 4 are inhomogeneously distributed across the substrate. Also apparent from Fig. 4 is that the density of the QD's is sharply diminished in regions where the large islands appear, which strongly suggests that the growth of the large islands proceeds at the expense of the QD's.

Due to the finite radius of the probe tip, AFM is not expected to yield an accurate representation of the true PSD of surfaces that contain small, high aspect ratio features such as quantum dots. Specifically the AFM can resolve the height of the dots, but not their lateral dimension. In addition to reducing the roll-off frequency associated with the dot diameter, the AFM also exaggerates the dot volumes, which increases the magnitude of the PSD associated with the dots. Compared to capped dot structures, which are amenable to TEM and cross-sectional STM analysis, the shape of uncapped InAs quantum dots is normally inferred from AFM and RHEED measurements, and remains an outstanding issue in the literature.[19,9,20]

Accordingly, we have undertaken a study of the AFM images in order to estimate the true size of the dots in these films. The results of this analysis for two representative QD's and one large island, all from the film in Fig. 3(c), are illustrated in Fig. 7, where we show AFM dot profiles acquired along the slow scan axis, approximately parallel with the [010] crystal direction. Consistent with the observation from AFM that the dots are isotropic, we have modeled each dot as a cone, whose cross section is shown in Fig. 7. The radius of the AFM probe tip (assumed to be spherical) and the aspect ratio of each dot were fitting parameters. The simulated profile produced with a 30 nm radius probe tip (solid line) is found to be in excellent agreement with the actual AFM profile (open circles) in all three cases. Although it was necessary to truncate some of the cones slightly in order to optimize the fits, the effect of the truncation on the inferred dot volume was found to be small (less than 6% larger than the corresponding nontruncated cone). We regard these fits as a reliable indicator of the actual tip radius. The manufacturer does not specify a typical tip radius, but indicates it is larger than 10 nm.

These results and the results of similarly good fits obtained for QD profiles along [100], with the same 30 nm tip radius, are summarized in Fig. 6(b). We note that the QD aspect ratio increases with dot height, which is consistent with a recent AFM study of InAs dots.[19] The smallest dots had aspect ratios corresponding to a $\sim 22°$ side inclination as shown in Fig. 7(a), which is close to the facet angle (25 °) of the $\langle 100 \rangle$ profiles of a {316}-faceted pyramid. The presence of these facets has been proposed to explain chevrons observed in RHEED patterns from InAs dots,[9] which we have also observed in our own QD growth experiments. Thus it is likely that the low aspect ratio dots include {316} facets. There is a systematic difference in the aspect ratios along the two orthogonal $\langle 100 \rangle$ directions in Fig. 6(b), which may reflect a real anisotropy in the dot shape, or it could be an artifact of the scanning process. We did not investigate this effect further. The true QD shape is almost certainly a faceted structure, with an aspect ratio that changes in discrete steps, as different facets become energetically favored. However, for the purposes of determining the dot volumes, each dot was assumed to be a symmetrical cone with an effective aspect ratio given by the linear fit in Fig. 6(b). We have also examined six of the large islands, and find that the aspect ratio is approximately 0.5 in all cases [Fig. 7(c)]. The same result was found for the ripened islands in Fig. 4. This indicates that the side inclination limits at 45 °, which would correspond to a pyramidal structure incorporating {110} facets.

In accordance with the above results, we have calculated a corrected PSD for the distribution of QD's in Fig. 3(b), obtained after each dot has been replaced by a symmetrical cone whose aspect ratio is determined from the linear fit in Fig. 6(b). To estimate the effect of the large islands, we performed the same procedure for the large island distribution in the AFM image used to calculate curve *a* in Fig. 5, after first removing the QD's. Consistent with the discussion above the aspect ratio was taken to be 0.5 for all the large islands. In order to correct for the difference between the density of large islands ($0.37\ \mu m^{-2}$) in the AFM image and the average density ($0.3\ \mu m^{-2}$) determined from many images, the PSD was multiplied by a factor $3/3.7 = 0.81$. This is justified if the large island distribution is approximately random, as discussed below.

Based on the analysis above, the PSD of the QD distribution and the large island distribution are given by curves *c*

and *d*, respectively, in Fig. 5. Again, the high-q rolloff in both cases is due to the finite island diameters. The large island PSD is approximately an order of magnitude lower than that of the QD distribution, over the spatial-frequency range accessible to the *in situ* measurement. Thus the total island PSD (not shown) is essentially indistinguishable from curve *c* in this plot. Note that this implies that the increase in the scattering signal in Fig. 1 is due almost entirely to the growth of the QD's. The total PSD can be estimated by adding curves *c* and *d* together, if correlations between the spatial distributions of the two populations are not important, which we feel is the case based on inspection of the AFM images. This sum is added to the PSD of the buffer layer (curve *b*) to obtain an estimate of the PSD of the total surface (curve *e*), which again neglects any correlations.[22] Note that the resulting PSD rises above the PSD of the buffer layer at $q \sim 25\ \mu\mathrm{m}^{-1}$, which explains why the light-scattering signals (Fig. 1) showed no increase below this spatial frequency.

Assuming the PSD of the GaAs buffer is a reasonable approximation to the PSD of the starting surface before the quantum dot growth, we can make an independent estimate of the final PSD after the growth using the light-scattering data in Fig. 1, which is normalized to the initial scattering from the buffer layer. The final scattering signal at each spatial frequency is multiplied by the corresponding value of the buffer layer PSD (straight line fit to curve *b*) to obtain an estimate of the final PSD. The results (open squares) agree reasonably well with the corrected PSD obtained from the AFM analysis (curve e), indicating that the correction procedure is valid. By contrast the agreement with the uncorrected AFM data is poor. The fact that the normalized light-scattering signals need only be multiplied by the PSD of the GaAs buffer to obtain the correct magnitude of the final PSD, further suggests that background scattering in the chamber was below the level of the scattering signal from the wafer.

The results above can be understood by considering that the Fourier transform of a distribution of identical islands is the product of the transforms of the individual island shape, and an array of unit volume δ functions that maps the island distribution. At spatial frequencies below the roll-off frequency associated with the island diameter, the magnitude of the island shape transform approaches the island volume. Thus the PSD at the spatial frequencies of interest is proportional to the square of the island volume. Furthermore, the PSD of a random distribution of unit volume δ functions is equal to $2n$, where n is the areal density. The PSD for a random distribution of islands may then be written as

$$\mathrm{PSD}(n,V) = 2n\langle V^2 \rangle \tag{3.1}$$

where the angular brackets $\langle\ \rangle$ denote an average over the size distribution.

Assuming conical islands (aspect ratio$=0.5$) the PSD of the large island distribution should be 49 nm^4 (for any q below the rolloff due to the island shape) based on Eq. (3.1) and the measured height distributions from AFM. This is in excellent agreement with the PSD obtained from the measured spatial distribution of the large islands (curve *d* in Fig. 5). The PSD is independent of q consistent with the fact that the large islands appear to be randomly distributed. The PSD obtained using Eq. (3.1) for the QD distribution is 1467 nm^4. This agrees reasonably well with the PSD for the QD's determined from the analysis above (curve *c* of Fig. 5), for spatial frequencies near $q \sim 100\ \mu\mathrm{m}^{-1}$. This spatial frequency corresponds to a lengthscale of ~ 63 nm which is close to the average dot spacing, $L_{\mathrm{avg}} = n^{-1/2} = 58$ nm. The PSD decreases slightly at lower q because the true distribution of the dots in this film is more uniform than a random distribution, on lengthscales larger than the average dot spacing.

We have also performed an analysis of the QD's and large islands for the film that was annealed for 25 min at 440 °C. Based on the AFM image of this film (Fig. 4), we find that over the range accessible to the *in situ* measurements, the PSD of the large islands is 1×10^5 nm^4. By contrast the contribution to the PSD from the QD's is only 100 nm^4. Thus the PSD associated with the large islands is three orders of magnitude higher than that of the QD's. Therefore, during the late stages of annealing the light-scattering signal is dominated by the contribution from the large islands.

C. Analysis of light-scattering data

In order to extract quantitative information from the *in situ* light-scattering data, it is necessary to relate the signals to the surface structure of interest, namely the size and density of the islands. In the following discussion we will use the term ''islands'' as a generic term for the large islands and the quantum dots together. From visual inspection of AFM images, the distribution of the islands does not appear to be correlated with the underlying surface structure of the GaAs buffer layer.[22] In this case we can subtract the initial scattering signal from the signal during the island growth, in order to obtain the contribution to the PSD from the islands. As discussed above the spatial distribution of the QD's is not perfectly random. Hence, the PSD during the growth of the QD's will have a q dependence determined in part by the spatial correlations in the location of the dots. Once the large (and more randomly distributed) islands appear, they will dominate the signal as they grow in size and consume the dots, so that the signals should become q independent in accordance with Eq. (3.1).

In Fig. 8 we show the time dependence on a log-log scale of the three scattering signals from Fig. 2 for the anneal at 400 °C, together with data acquired during a similar experiment conducted at a temperature of 280 °C. The InAs from the first growth was removed by evaporation at 500 °C between the experiments, so that both sets of data could be obtained on the same sample during a single MBE run. Although all the samples discussed in this paper were prepared under nominally the same conditions, the growth conditions for these two experiments that were prepared during the same run are likely to be much closer to being identical. Some run-to-run variations in As_2 over-pressure and In flux are inevitable. The times t_o in this plot are 0.3 min and 1 min for the growths at 400 °C and 280 °C, respectively, which correspond to the times at which the 2D to 3D islanding transition was observed by RHEED. In order to extract the time evolution of the islands from the total light-scattering signal which includes the buffer layer, the initial scattering

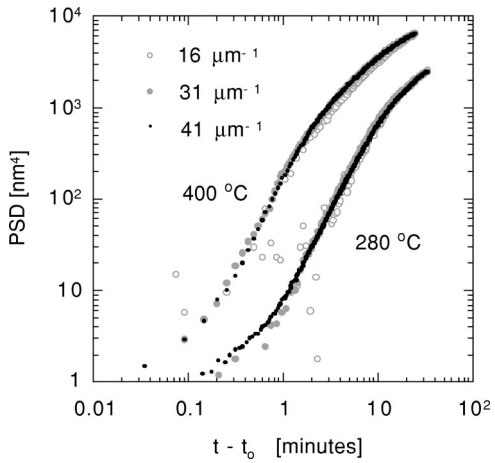

FIG. 8. Comparison of the q dependence of the scattering data in Fig. 2 for the 400 °C growth and annealing experiment, and a similar experiment performed during the same MBE run on the same buffer layer, at 280 °C. The initial background scattering due to the buffer layer has been subtracted from each signal, and the three scattering signals from each experiment are normalized to coincide at the end of the anneal. In this figure, the PSD has been calculated from the scattered light intensity based on an absolute calibration of the 41 μm^{-1} signal as discussed in the text.

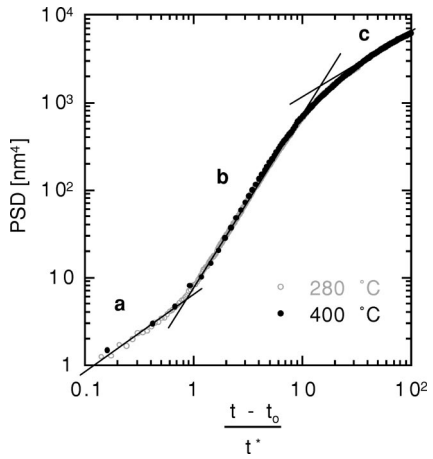

FIG. 9. Collapse of the two data sets in Fig. 8, obtained by rescaling the time axis for each temperature. The times, t^* used to obtain the data collapse were 0.2 and 1 min, respectively, for the films annealed at 400 and 280 °C. The three linear regions, which correspond to regions of distinct power-law behavior, have slopes of (a) 0.9, (b) 2.0, and (c) 0.75.

from the buffer layer has been subtracted as discussed above. The signals are then normalized so that they coincide at the end of growth.

Based on an absolute calibration of the 41 μm^{-1} signal in Fig. 8 we have calculated the PSD from the scattered light intensity at this spatial frequency. We obtained the optical prefactors needed to compute the PSD by placing a Lambertian scattering surface at the sample position. This calibration, which is believed to be accurate to a factor of about 2, could not be performed for the other two signals due to run-to-run variations in optical alignment. However the scale on the vertical axis should be correct for all three signals if the final PSD is q independent, consistent with our AFM measurements on the large islands. We note that at long times when all three signals at different spatial frequencies are strong, there is no significant difference in the ratios of the three signals at either temperature as a function of time, indicating that the spatial frequency dependence of the PSD is not changing. This would be true if, for example, the islands were randomly distributed and remained random during the annealing. From this and similar results obtained on other growths, we conclude that the signal at any q is proportional to $n\langle V^2\rangle$ throughout the late stages of the anneal, which we associate with the growth and ripening of the large randomly distributed islands. The signal-to-noise ratio in the data is not good enough to determine the time dependence at each q during the initial stage when the quantum dots are growing.

We can further simplify the interpretation of the data if the relative size fluctuation of the islands, $\sigma_v/\langle V\rangle$ is constant, where σ_v is the standard deviation of the volume.[20] In this case, Eq. (3.1) may be written

$$\mathrm{PSD} \sim 2n(\langle V\rangle^2+\sigma_v^2) \sim 2n(k+1)\langle V\rangle^2, \tag{3.2}$$

where $k=(\sigma_v/\langle V\rangle)^2$ and the proportionalities may be replaced by equalities if the island distribution is random. We have calculated the average dot sizes and variances using the height distributions from AFM discussed above, as well as those from a similar analysis of the large islands in Fig. 4. A conical dot geometry was assumed in all cases. We find that k is small (<0.2) for both the QD's and the initial large islands in Fig. 3(c), consistent with a narrow size distribution. However, the value of k associated with the large islands appears to increase at the late stages of annealing, to ~ 0.7 according to Fig. 4. This broadening of the relative size distribution reflects the inhomogeneity in the ripening process across the film, which is visible in the AFM image. In light of Eq. (3.2), the effect of assuming a constant k is to underestimate the volume during the final stages of ripening by a factor of about $(1.7/1.2)^{1/2} \sim 1.2$, which is negligible for the discussion here. Therefore, the time dependence of the light-scattering signal after the large islands have nucleated is well approximated by

$$I(t)-I_o \sim \mathrm{PSD}(t) \sim n(t)\{\langle V\rangle(t)\}^2, \tag{3.3}$$

where $I(t)$ is the scattered light intensity, at any spatial frequency, and I_o is the initial scattering intensity. Equation (3.3) also applies to the growth of the QD's, however, due to the observed deviation of the QD distribution from a random distribution the PSD will have a q dependence that may depend on t.

IV. DISCUSSION

The data in Fig. 8, acquired during two growths at considerably different temperatures (400 °C and 280 °C), display a time dependence that is strikingly similar. The simplest interpretation is that the main effect of an increase in temperature is to increase the diffusion rate for atoms on the surface, thus rescaling the time for the island formation and growth processes. Accordingly, in Fig. 9, we have replotted the data corresponding to $q=41$ μm^{-1}, using a renormalized time axis. The two curves, obtained using a renormalization time, t^* of 1 min and 0.2 min for the growths at 280 and 400 °C, respectively, are seen to coincide almost per-

fectly during the entire time of the anneal. This result is quite remarkable, given that other than t^*, there are no fitting parameters. We emphasize that in order to reproduce the growth conditions (other than the temperature) as closely as possible, both growths were performed on the same buffer layer during the same MBE run. The striking collapse of these two data sets supports the conclusion that given identical growth conditions, the effect of temperature on the dynamics of the island growth during annealing is simply to rescale the time axis. Three regions of distinct time dependence emerge in Fig. 9, labeled a, b, and c, which exhibit different power-law behavior. We associate each of these regions, respectively, with nucleation of the initial distribution of QD's (a), growth of the large islands at the expense of the QD's (b), and Ostwald ripening of the large islands after the QD density has been substantially reduced (c).

As we discuss further below, the approximately linear increase of the scattering signal with time in region a of Fig. 9 is associated with the growth of the QD's. The more rapid increase in region b is attributed to the emergence of the larger islands. These islands grow initially at the expense of the QD's, which act as a source of material for the growing islands as discussed above. Thus the simplest applicable model is that of 2D diffusion-limited growth from a ''vapor'' of unattached atoms on the surface, for which the island volume should increase linearly with time.[12] According to Eq. (3.3) the observed slope of 2 in region b is consistent with this mechanism, provided the density of large islands remains fixed. This is reasonable if the large islands consume the quantum dots, since the nucleation rate would be expected to drop off rapidly as the islands grow and reduce the QD density.

As shown in Fig. 4, the QD population is depleted in regions where the large island density is high, presumably because the QD's have been consumed by the large islands. In order for the islands in these regions to continue to grow they must compete with each other for material, which is Ostwald ripening. For the case of ripening limited by 2D surface diffusion, the average island size will increase as $t^{3/4}$, and the density must decrease as $1/\langle V\rangle$ to conserve material.[11,12] Hence a $t^{3/4}$ dependence is expected for the PSD at long times, which is consistent with the data in region c as shown in Fig. 9.

The initial time dependence (region a of Fig. 9) is sensitive to the value of t_o. It was, therefore, necessary to adjust t_o in each case so that the initial behavior followed a power law (i.e., constant slope in Fig. 9); however, as mentioned previously the fitted t_o was found in each case to match the time of the 2D-to-3D transition observed by RHEED. Using this procedure we find an initial time dependence that is approximately linear (slope 0.9 in Fig. 9). Further evidence of this behavior is shown in the inset of Fig. 1. Here we plot the 41 μm^{-1} signal for the growth at 490 °C on a log scale, using a t_o of 0.2 minutes in agreement with the RHEED transition. Again, we have subtracted the background scattering signal and calculated the PSD from this signal based on the calibration described previously. The time-dependence of the PSD, which is seen to be approximately linear throughout this experiment, is relatively insensitive to the choice of t_o for times greater than 0.5 minutes. Furthermore, for this sample, the scattering from the large islands is expected to account for less than 10% of the total signal according to the AFM analysis carried out on the quenched sample. Therefore, the order-of-magnitude increase in the PSD must be due to the formation of the QD's. Hence, we conclude that the initial increase in the PSD associated with the QD growth is approximately linear with time. It is not clear whether this initial time dependence is due to a change in the dot density or the average dot size, or both. Since the size of the quantum dots is observed to saturate during annealing it is tempting to attribute the linear increase in scattering to the continuing nucleation of uniform-size dots from the wetting layer.

It is interesting that the signal in the inset of Fig. 1 cannot be made to coincide with the curves in Fig. 9 with a simple rescaling of the time axis. In particular, the signal in Fig. 1 grows linearly with time until the end of growth, by which time the PSD has reached a value of ~ 200 nm^4. By contrast the signals in Fig. 9 switch from a linear time dependence to a t^2 dependence by the time the PSD has reached a value of only ~ 10 nm^4. This implies that the emergence of the large islands was delayed in the growth in Fig. 1. We attribute this effect to differences in growth conditions, since the growth in Fig. 1 was carried out during a different MBE run and on a different substrate than the growths in Fig. 9. Arsenic overpressure in particular is known to play an important role in the growth of InAs QD's.[5]

Finally, it is noteworthy that the signal does not saturate at any point during the growth of the QD's, which would be a direct indication of self-limiting behavior. Possibly in our experiments the saturation is masked by the emergence of large islands. In order to be more definitive it would be desirable to monitor the time evolution of the quantum dots under conditions where large islands do not nucleate during annealing.

V. CONCLUSIONS

In conclusion, we have shown that ultraviolet light scattering can detect the onset of quantum dot formation in real time, in the InAs/GaAs system. The *in situ* light-scattering results are found to be in good agreement with the island size distributions determined from AFM, taking into account the finite radius of the probe tip. We explain the time evolution of the scattering signal during annealing in terms of a three-stage process in which the quantum dots nucleate and grow, large islands nucleate and consume the quantum dots, and the large islands ripen in a manner consistent with 2D diffusion-limited Ostwald ripening. For growths performed under nominally identical conditions during the same MBE run, the temperature dependence of these processes is found to be accounted for by a simple rescaling of the time axis.

ACKNOWLEDGMENT

We thank the NSERC for financial support.

*Also at Department of Electrical and Computer Engineering, University of British Columbia, Vancouver, Canada.

[1] E.L. Church, H.A. Jenkinson, and J.M. Zavada, Opt. Eng. (Bellingham) **16**, 360 (1977).

[2] T. Pinnington, C. Lavoie, T. Tiedje, B. Haveman, and E. Nodwell, Phys. Rev. Lett. **79**, 1698 (1997).

[3] J.A. Floro, G.A. Lucadamo, E. Chason, L.B. Freund, M. Sinclair, R.D. Twesten, and R.Q. Hwang, Phys. Rev. Lett. **80**, 4717 (1998).

[4] S. Fafard, Z.R. Wasilewski, C. Nì Allen, D. Picard, P.G. Piva, and J.P. McCaffrey, Superlattices Microstruct. **25**, 87 (1999).

[5] R. Leon, C. Lobo, J. Zou, T. Romeo, and D.J.H. Cockayne, Phys. Rev. Lett. **81**, 2486 (1998).

[6] R. Heitz, T.R. Ramachandran, A. Kalburge, Q. Xie, I. Mukhametzhanov, P. Chen, and A. Madhukar, Phys. Rev. Lett. **78**, 4071 (1997).

[7] S.R. Johnson, C. Lavoie, T. Tiedje, and J.A. MacKenzie, J. Vac. Sci. Technol. B **11**, 1007 (1993).

[8] A. Wankerl, A.T. Schremer, and J.R. Shealy, Appl. Phys. Lett. **72**, 3332 (1998).

[9] H. Lee, R. Lowe-Webb, W. Yang, and P.C. Sercel, Appl. Phys. Lett. **72**, 812 (1998).

[10] P.R. Spyak and W.L. Wolfe, Opt. Eng. (Bellingham) **31**, 1746 (1992).

[11] M. Zinke-Allmang, L.C. Feldman, and S. Nakahara, Appl. Phys. Lett. **51**, 975 (1987).

[12] B.K. Chakraverty, J. Phys. Chem. Solids **28**, 2401 (1967).

[13] B.D. Min, Y. Kim, E.K. Kim, S-K Min, and M.J. Park, Phys. Rev. B **57**, 11 879 (1998).

[14] C. Lavoie, T. Pinnington, T. Tiedje, J.L. Hutter, G. Soerensen, and R. Streater, Can. J. Phys. **74**, S49 (1996).

[15] M.K. Nissen, C. Lavoie, S. Eisebitt, T. Pinnington, and T. Tiedje, Scanning Microsc. **8**, 935 (1994).

[16] J. Aué and J.Th.M. De Hosson, Appl. Phys. Lett. **71**, 1347 (1997).

[17] A. L. Barabási, *Fractal Concepts in Surface Growth* (Cambridge University Press, Cambridge, 1995).

[18] F.M. Ross, J. Tersoff, and R.M. Tromp, Phys. Rev. Lett. **80**, 984 (1998).

[19] H. Saito, K. Nishi, and S. Sugou, Appl. Phys. Lett. **74**, 1224 (1999).

[20] Experimental evidence that k is constant for QD distributions in the InAs/GaAs system is presented in Y. Ebiko, S. Muto, D. Suzuki, S. Itoh, K. Shiramine, T. Haga, Y. Nakata, and N. Yokoyama, Phys. Rev. Lett. **80**, 2650 (1998).

[21] S. Lee, I. Daruka, C.S. Kim, A.-L. Barabási, J.L. Merz, and J.K. Furdyna, Phys. Rev. Lett. **81**, 3479 (1998).

[22] One source of correlation between the substrate structure and the dot location is dot alignment along step edges, however AFM images show that this is not an important effect in our films.